Contents lists available at Science-Gate

International Journal of Advanced and Applied Sciences

Journal homepage: https://www.science-gate.com/IJAAS.html

Multiple-constraint-based coronary artery disease detection via image segmentation using Spider U-Net with hybrid pre-processing techniques

Sarwar Shah Khan [1,*], Yasser Alharbi [2]

[1]Department of Computer Science, Iqra National University, Swat Campus, Pakistan
[2]College of Computer Science and Engineering, University of Hail, Hail, Saudi Arabia

ARTICLE INFO

Article history:
Received 21 March 2026
Received in revised form
21 August 2026
Accepted 19 September 2026

Keywords:
Invasive coronary angiography
Coronary artery disease
Blood vessel segmentation
Image preprocessing
Deep learning

ABSTRACT

The role of coronary angiography is important for visualizing coronary arteries and detecting abnormalities such as coronary artery disease (CAD). Nevertheless, its diagnostic value is often constrained by image noise, poor contrast resolution, motion artifacts, and changes in vessel curvature and orientation. To overcome these challenges, this study proposes an automated CAD segmentation and diagnosis system using angiographic X-ray images (invasive coronary angiograms). The proposed framework begins with an image preprocessing step using two hybrid noise reduction and contrast enhancement algorithms, namely, the Median Filter with Optimized Maximum Contrast and the Adaptive Median Filter with Optimized Maximum Contrast, to reduce noise without losing edge information. For coronary artery segmentation, a Spider U-Net is adopted, which complements the traditional U-Net with attention mechanisms to enhance feature saliency and focus on clinically significant regions. The proposed framework is evaluated using several statistical measures, with accuracy, precision, recall, F1-score, and Jaccard similarity coefficient values of 0.9549, 0.8510, 0.7836, 0.9008, and 0.8762, respectively. The experimental results demonstrate that the proposed framework outperforms existing methods by effectively reducing background artifacts and enhancing the clarity and precision of vascular structures, thereby improving the reliability of coronary artery disease diagnosis.

© 2026 The Authors. Published by IASE. This is an open access article under the CC BY-NC-ND license (https://creativecommons.org/licenses/by-nc-nd/4.0/).

1. Introduction

Angiographic images play an important role in medical imaging due to their ability to visualize blood vessels and assist in the diagnosis of vascular abnormalities. Angiography is a medical imaging procedure that enables physicians to examine the internal structure of circulatory vessels, including arteries, veins, heart chambers, and associated organs. It is commonly used to detect conditions such as internal bleeding, aneurysms, and other vascular abnormalities. Angiography is an important diagnostic tool, as it is widely used for the diagnosis of various vascular disorders. Furthermore, it facilitates the planning of treatment and intervention for complications, such as blockages, constriction, and other defects of vital organs such as the heart, brain, and retina (Vilimek et al., 2022). Abnormal blood circulation may have an undesirable effect on the organs that depend on these vessels to circulate, which may cause severe health problems, including heart attack, angina, stroke, and other complications. Angiography involves the use of X-rays to visualize the flow of blood in the arteries of the human body to detect the presence of abnormalities in the vessels. It is most often believed to be a safe procedure, and it has great advantages to the patients subjected to it (Balasamy and Shamia, 2023). A particular method of angiography is known as coronary angiography, and this is used to visualize the coronary arteries, which supply blood to the heart muscle (Verma et al., 2015). Nevertheless, there are some difficulties associated with the detection of coronary artery disease using a coronary angiogram, such as image noise, low contrast, respiratory motion artifacts, and changes in the orientation of the vessels (Ning et al., 2009).

It is observed that digital images are extensively utilized in numerous areas, and medical analysis of images is one of the most striking ones. One of the fields of the medical image processing domain is the

* Corresponding Author.
Email Address: sarwarshah@inu.edu.pk (S. S. Khan)
https://doi.org/10.21833/ijaas.2026.09.010
Corresponding author's ORCID profile:
https://orcid.org/0000-0002-6387-4114
2313-626X/© 2026 The Authors. Published by IASE.
This is an open access article under the CC BY-NC-ND license (https://creativecommons.org/licenses/by-nc-nd/4.0/)

acquisition of medical images, processing them when necessary, and generating a processed image as a diagnostic or analytical result. Even though medical images are usually processed directly, they can frequently be pre-processed before processing in order to enhance the overall quality of the image with denoising and contrast-enhancing tasks (Balasamy and Shamia, 2023; Vilimek et al., 2022). Interest in the field of better disease diagnosis through the quality of medical images is high among both researchers and clinicians, and image enhancement offers much assistance in this context by minimizing visual distortions and enhancing contrast (Verma et al., 2015).

Blood vessel segmentation in coronary angiography images is relevant in the evaluation of the severity of vascular disorders. It assists doctors with accurate diagnosis, planning of treatment, and three-dimensional representations of blood vessels to enhance visualization and analysis (Balasamy and Shamia, 2023). An accurate segmentation output can reduce the time physicians spend on segmentation by hand and enhance the accuracy of the diagnosis. The extracted blood vessels can also be utilized as a foundation for studies that can be conducted later, such as showing the velocity of the blood flow and the extent to which the vessel is narrowed (Verma et al., 2015).

Existing methods suffer from poor vessel boundary detection under noise, low contrast, and anatomical variability. This research aims to improve the identification of coronary artery disease through developing a new segmentation framework. The coronary artery disease detection involves two major stages, which are the pre-processing of the image data and the segmentation of the particular areas.

Noise reduction and low-contrast enhancement are particularly related to the pre-processing of the coronary angiograms. Further examination and diagnosis of image quality enhancement methods are conducted in this article through several approaches. When applied in the case of coronary angiography, the paper aims to enhance the accuracy and dependability of subsequent processing and analysis procedures by addressing the problem of low-contrast or noisiness detection, to the effect that pre-processing must be performed initially. The importance of image segmentation of such coronary angiography images is that it can influence disease detection and improve clinical decision-making. Image segmentation enhances visualization through the separation of blood vessels and other tissues in the body and the identification of constricted or occluded blood vessels. It may assist in proper diagnosis, aid in stenosis classification, and enhance treatment plans, namely stenting or bypass surgery. Image segmentation will aid in working less to manually segment the image, give the quantitative values of the vessels' characteristics, increase 3D reconstruction and anatomical visualization, and improve the AI-based diagnostic algorithms to detect CAD automatically. All these improvements enhance the efficiency, accuracy, and patient outcomes in the diagnosis of coronary artery disease.

The objective of medical image enhancement is to make medical images more visible and clearer, and to enhance details in medical images to reveal more features that are important to the diagnosis; hence, a more accurate and reliable diagnosis can be made. Highlights of the main contribution are:

- This study proposed a novel framework based on the Spider-U-Net architecture to accurately extract coronary artery vessels and ensure comprehensive segmentation of all arteries within the image. In addition, the identification of vessel structures is refined to enhance the accuracy of segmentation.
- Preprocessing is an important step to analyze and ensure the quality of coronary angiography images, with an emphasis on addressing structural constraints of the coronary arteries. Key constraints considered include noise removal and low-contrast enhancement.
- This study proposes novel hybrid approaches in medical image processing by combining denoising techniques with image contrast enhancement. Specifically, it introduces the Median Filter with Optimized Maximum Contrast (MF+OMC) and the Adaptive Median Filter with Optimized Maximum Contrast (AMF+OMC).

2. Literature review

This section is divided into two main subsections: the first discusses multiple constraints and pre-processing techniques, while the second focuses on coronary artery segmentation and the detection of CAD using X-ray angiography. Through this analysis, a research gap was recognized, emphasizing the necessity for a more advanced model to enhance the accuracy of CAD detection.

Over the past few years, the analysis and interpretation of medical images have become a highly significant field of study in academia. Mainly focusing on two key areas, enhancing visual clarity and addressing problems related to low-contrast regions has gathered substantial interest from researchers. A summary of related work focused on denoising and improving contrast in medical imaging is presented in Table 1.

In the past couple of decades, medical imaging, especially in different types of angiographies, has received much attention with regard to the segmentation of blood vessels. It was a useful technique for improving the quality of clear medical images and hence for more accurate clinical examinations and reliable diagnostic outcomes.

Two adversarial networks are trained together in a self-supervised framework—one focused on extracting blood vessels from cardiac angiography images, and the other responsible for creating artificial vascular structures on masked image frames. The model trained through this approach is later used in various vessel segmentation tasks, relying on the vessel features it has already learned.

Additionally, a fractal-based synthetic module is introduced to support self-supervised learning without the need for manually labeled vessel maps (Ma et al., 2021). CNNs are very useful tools for the automatic extraction of specific attribute sets from adequate quantities of labeled training data. The employed CNN architecture is expected to learn attributes through which vascular regions in an angiography can be identified (Huang et al., 2018).

Table 1: Summary of the literature review

Reference	Dataset	Approaches	Performance measures	Outcomes
Vilimek et al. (2022)	Ultrasound images	Wavelet transform	SSIM, CoC, MSE, PSNR	0.726, 0.919, 9.68, 31.43
Balasamy and Shamia (2023)	MRI image	Switched mode fuzzy median filter	PSNR, NC	49.0021, 0.9970
Verma et al. (2015)	MRI image	Adaptive median filter	PSNR, SNR	23.9323, 14.4522
Ning et al. (2009)	CT, MRI images	Median filter, adaptive median filter	PSNR	12.5896, 9.4984
Chen et al. (2019)	X-ray, ultrasound, CT scan, MRI images	Discrete wavelet transform, median filter	PSNR, SNR	25.4350, 6.8040
Huang and Wan (2020)	General images	Total variation	MSSIM, SNR	0.8436, 25.6228
Sagar et al. (2020)	MRI images	Circular adaptive median mask	PSNR	28.7718
Arulpandy and Pricilla (2020)	MRI images, general images	Modified mean mask	PSNR, MSE	11.5127, 0.1263
Showkat et al. (2021)	MRI images	Contrast stretching	PSNR, SSIM	16.24, 0.9932
Agarwal et al. (2020)	MRI images	Histogram equalization	PSNR, MSE	29.07, 80.92
Dar and Mittal (2021)	Digital images	Adaptive histogram equalization	PSNR, NAE	53.4047, 1.0267
Wang et al. (2020)	CT	Chaos-based optimization	Entropy, Edge contents	6.65, 0.19

U-Net is one of the most well-known and successful neural network architectures and is widely used for biomedical image segmentation. Four deep learning architectures for semantic segmentation were designed based on the U-Net architecture. Each architecture has an encoder in the form of a fully convolutional backbone and a decoder implemented using deconvolutional layers to recover the segmented output. ResNet (He et al., 2016), DenseNet (Huang et al., 2017), and Residual Attention Network (Wang et al., 2017) were used for image classification, respectively. Subsequently, these deep learning architectures were evaluated for their performance in segmenting X-ray angiographic images (Xian et al., 2020).

A coarse-to-fine strategy is adopted for the extraction of coronary arteries. The authors introduced a new method to compute the intersection points of primary and secondary coronary arteries accurately. They also present a U-Net algorithm tailored for the first segmentation of the central coronary arteries (Thuy et al., 2021).

T-Net, a recently introduced nested encoder-decoder model, is constructed from several small encoder-decoder modules placed within every block of a convolutional network. In contrast to the U-Net, in which there is a sole path of connection between encoder and decoder layers, the T-Net addresses this constraint by adding several interconnected modules inside the network, improving information transfer between layers (Jun et al., 2020). The Sequential Vessel Segmentation Network is a deep network encoder-decoder network structure that segments 2-Dimensional vessel masks of the current frame. It integrates a channel attention mechanism in the decoder, promotes skip connections with feature fusion, and conducts temporal-spatial feature extraction in the encoder (Hao et al., 2020).

To segment blood vessels from both coronary angiograms and retinal fundus images, a common VSSC-Net is employed after dedicated pre-processing for each imaging modality. This network has two dedicated vessel extraction layers based on a VGG-16 backbone with extra supervisory feedback. These layers contain vessel-specific convolutional blocks to identify vascular structures precisely, skip-chain convolutional layers to promote efficient feature flow, and a unique feature map summation technique to combine learned representations (Samuel and Veeramalai, 2021).

3. Proposed methodology

In this study, X-ray angiogram images were employed in the detection of coronary artery disease. In order to do this, two major operations are used: image pre-processing and extraction of the coronary artery vessels (segmentation) (Khan et al., 2023a). Each of the steps used is explained in greater detail below, and the entire process of the proposed architecture of the framework is represented in Fig. 1.

3.1. Preprocessing

The issues related to low contrast, background noise, non-uniform pixel distribution, low-quality vascular structures, and excess artifacts were resolved at this stage. In order to approach such issues well, different restrictions were critically considered, and suitable adjusting procedures were implemented (Khan et al., 2023b).

3.1.1. Median filter (MF) noise removal approach

The Median Filter is a method that is used to eliminate noise, and a specific pixel in a given window is substituted with the median of the intensity values within the window. The method is particularly effective in removing noise without removing significant details, as well as keeping edges. The target pixel (Px) is surrounded by a

square-shaped window, which is determined by predefined width and height dimensions, and therefore makes the filter act locally about each pixel.

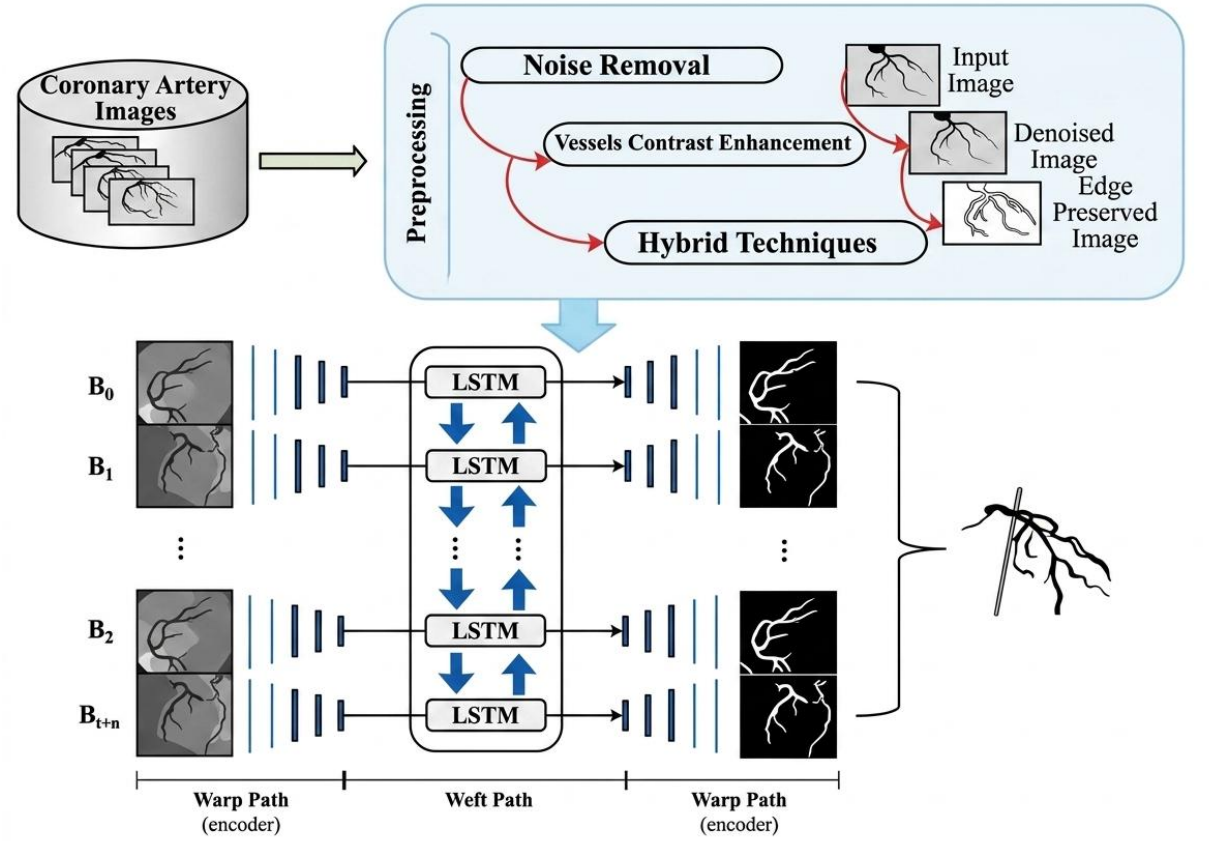


Fig. 1: Proposed framework systematic architecture

When the image is colored, the median is taken independently in each channel (e.g., Red, Green, and Blue). The pixel intensity values of each channel within the given window are gathered, and the median of the values is calculated. The median, which is channel-specific, is then put in the central pixel Px. The process is used individually in all the color channels to maintain consistency in colors and minimize noise. In mathematical notation:

- I(a, b) Denote the intensity value of pixel Px at position (a, b).
- W be the window size (odd sizes are desirable for symmetry).

The median value Med of the pixel intensities in the window is computed as:

$$\text{Med} = \text{Median}(\text{I}(\text{a} - \text{i}, \text{b} - \text{i}) | \text{i} = -\text{x to x}, \text{J} = -\text{x to x}) \quad (1)$$

where, $'x'$ is defined as the integer result of $(w - 1)/2$, specifying the neighborhood range around the target pixel Px. The 'Median' function then selects the middle value from this localized set of pixel intensities.

Once the median value, denoted by Med, is determined, it replaces the intensity of the target pixel Px. The MF is considered a robust technique of noise reduction since it replaces every pixel brightness intensity with the median value in its neighborhood. This process effectively removes unwanted noise without affecting image edges and fine details.

3.1.2. Adaptive median filter (AMF) noise removal approach

AMF is a denoising method that changes the size of the window according to the local features of the image. It is quite effective in eliminating noise contained in images when there is a sharp difference in noise and signal intensity.

Unlike the other filters with a fixed window size, the AMF varies the size of the window with the characteristics of the local area, typically around the pixel under consideration. The algorithm identifies the median pixel intensity of the pixel intensities in the adaptive window and replaces the pixel intensity with the median.

The algorithm internally adapts the window size to the alterations in the local image content. The process starts with a small kernel to retain information and changes the window size when the median is not changed. It ensures noise is removed and edges and primary features are retained. The Adaptive Median Filter is best suited for images with

irregular levels of noise since it changes its behavior in the direction of the changing noise pattern. However, it may not be as effective in removing noise that is uniformly distributed throughout the image.

3.1.3. Optimized maximum contrast (OMC) contrast enhancement approach

The OMC technique is designed to enhance image contrast by stretching its dynamic range. It works by adjusting the pixel intensity values in a way that preserves their relative differences, making the image appear sharper and more informative. This method is particularly effective for images where the intensity values are closely packed within a limited range. In mathematical terms, the approach can be expressed as follows. The intensities in an image generally span from 0 to $L-1$, where L denotes the number of possible intensity levels—for an 8-bit image, this is typically 256. Histogram equalization (HE) is used to enhance contrast and distribute the intensity values in the given image. The HE function H(v) can be computed as the histogram CDF function:

$$H(v) = \frac{CDF(v) - CDF_{min}}{1 - CDF_{min}} \quad (2)$$

where, v is the intensity value, CDF(v) is the cumulative distribution function value of v, and CDF_{min} is the minimal CDF value.

The OMC method includes a transformation function T(v) that remaps the increased brightness to its optimum values. It can be given as:

$$T(v) = \gamma . H(v) + \delta \quad (3)$$

where, γ and δ variables control the contrast refinement. γ determines the slope of the transformation and, therefore, the amount of refinement, and δ determines the shift and, consequently, the level of minimal brightness.

The transformed brightness values are found by applying the transformation function to the intensity value of every pixel of the input image.

$$I_{enhanced}(x, y) = T(I_{enhanced}(x, y)) \quad (4)$$

By varying the γ and δ variables, you can regulate the amount of contrast refinement. A higher γ will increase the total contrast, and varying δ will regulate the intensity of the improved image.

OMC maximizes the contrast and tries to maintain the intensity relationships. This method is useful in cases where the true image lacks much intensity because of a low range of brightness values.

3.1.4. Median filter with optimized maximum contrast (MF + OMC)

The (MF + OMC) hybrid method integrates the denoising properties of the MF with the improved contrast properties of the OMC method. This hybrid method seeks not only to minimize noise in the angiogram but also to maximize its contrast for improved visual appearance.

The MF is used on the input image to eliminate noise. The MF substitutes every pixel value with the median of neighboring pixels within a specified window. Suppose $x(r, s)$ is the brightness value of the pixel at position (r, s) in the input image, and $y(r, s)$ is the brightness value of the corresponding pixel in the output (denoised) image after MF.

$$y(r, s) = \text{med}\{x(u, v): (u, v) \text{is in the neighborhood of } x(r, s)\} \quad (5)$$

The OMC enhancement technique is employed on the denoised image using the Median Filter to enhance its contrast through Eq. 3.

The resulting image is achieved by applying the transformation function to every pixel's brightness value in the noise-reduced image after MF with:

$$I_{enhanced}(r, s) = T\big(x(r, s)\big) \quad (6)$$

By integrating the MF with the OMC method, the hybrid approach efficiently denoises the image through the use of the MF and subsequently improves the contrast of the denoised image through the Optimized Maximum Contrast method. This results in a less noisy image with enhanced contrast, resulting in enhanced visual quality. Algorithm 1 outlines the precise series of steps carried out to put into practice the MF+ OMC hybrid technique.

3.1.5. Adaptive median filter with optimized maximum contrast (AMF + OMC)

The (AMF + OMC) hybrid method integrates the denoising features of the AMF with the improved contrast features of the OMC method. The hybrid method seeks to minimize the noise in the image while improving its overall contrast for enhanced visual appearance.

The AMF is used on the input image to reduce noise. The AMF adapts the size of the filter window according to the local properties of the image. It replaces each pixel value with the median value of the neighboring pixels in a variable window.

Let $f(a, b)$ be the brightness of the pixel at the position (a, b) in the input image, and $g(a, b)$ be the brightness of the corresponding pixel in the output (denoised) image after Adaptive Median Filtering.

$$g(a, b) = \text{Median (pixels in a afaptive window center redat } (a, b) \text{ e} \quad (7)$$

After applying the Adaptive Median Filter (AMF), the Optimized Maximum Contrast (OMC) method is used to improve the contrast of the filtered image, as described in Eq. 3. The output image is achieved by applying the transformation function to every pixel

brightness value of the denoised image, following AMF via Eq. 6.

By utilizing the (AMF + OMC) algorithm together, the hybrid method successfully removes noise from the image with the AMF and later increases the contrast of the denoised image with the OMC algorithm. The end product is an image with better image quality, as noise is minimized and contrast is increased. Algorithm 2 presents the precise order of operations in applying the AMF+OMC hybrid method.

Algorithm 1: Median filter with optimized maximum contrast (MF + OMC)

Input: Image A^{ip}
Parameters:
- Filtered Image (f^i) *of MF*
- Window Size (W^s)
- Denoised Pixel Value (M)
- Alpha (α) *value for the OMC*
- Beta (β) *value for the OMC*
- Enhanced Pixel Value ($v_{enhanced}(p)$)
Step 1: Apply a Median Filter
For *"each pixel (x,y) in the image* A^{ip} *//This is for loop*
Extract the pixel values at (x,y)"
Compute the median $M(x, y)$ *using Eq. (1)*
end for
$f^i = MF(A^{ip}, W^s(n \times n))$
Step 2: Apply Optimized Maximum Contrast Enhancement
α = *Choose* α *Value*
β = *Choose* β *Value*
Compute OMC using Eq. (3)
Step 3: Enhance the Denoised Image
For *each pixel (x, y) in* f^i *//This is for loop*
$M = f^i(x, y)$
$v_{enhanced}(p) = \alpha * M + \beta$
$I_{enhanced}(x, y) = v_{enhanced}(p)$ *using Eq. (4)*
end for
Step 4: Output Enhanced Image using Eq. (6)

3.2. Spider U-Net model

The Spider U-Net model is a development based on the initial U-Net model, which has been applied extensively for image segmentation (Lee et al., 2021). The word "Spider" in Spider U-Net is used to refer to the spider web-like connections in the network engineered to capture cryptic spatial relationships in medical images. Spider U-Net (Lee et al., 2021) is designed to capture in detail information about blood vessels by merging spatial information and inter-slice connectivity into each warp path and weft path, in the same way that one weaves a web of cloth. This is achieved by a process that can be likened to three stages. First, the encoder section of the warp path generates spatial features from a sequence of images of a fixed length. Secondly, the path of weft is intertwined with the path of warp, facilitating information flow that passes through successive images. It then applies the use of Long Short-Term Memory as a means of tapping into the inter-slice connection of blood vessels. Lastly, the decoder component of the path of warp relies on augmented rich information, e.g., inter-slice connectivity, to accurately approximate the segmentation mask. The Spider U-Net model is presented to describe such steps.

Algorithm 2: Adaptive median filter + optimized maximum contrast (AMF + OMC)

Input: *Image* A^{ip}
Parameters:
- Filtered Image (f^i) *of AMF*
- Window Size (W^s)
- Denoised Pixel Value (M)
- Alpha (α) *value for the OMC*
- Beta (β) *value for the OMC*
- Enhanced Pixel Value ($v_{enhanced}(p)$)

Step 1: Apply Adaptive Median Filter
$W^s \leftarrow S_{min} \& S_{max}$
For *each pixel (x, y) in the image* A^{ip} *//This is for loop*
$W^s \leftarrow S = S_{min}$
While $S <= S_{max}$: *//This is while loop*
Extract pixel values $W^s S_{centered}(x, y)$
Compute the median $M(x, y)$ *using Eq. (1)*
Compute local dynamic range $L(x, y) = max_{\{pixelvaluesinwindow\}} - min_{\{pixelvaluesinwindow\}}$
If $M(x, y)$ *is within* $L(x, y)$, *set* $E(x, y) = M(x, y)$. *//This is IF Statement*
Otherwise, increment S and repeat the While loop
end while
end for
Step 2: Apply Optimized Maximum Contrast Enhancement
α = *Choose* α *Value*
β = *Choose* β *Value*
Compute OMC using Eq. (3)
Step 3: Enhance the Denoised Image
For *each pixel (x, y) in* f^i *//This is for loop*
$M = f^i(x, y)$
$v_{enhanced}(p) = \alpha * M + \beta$
$I_{enhanced}(x, y) = v_{enhanced}(p)$ *using Eq. (4)*
end for
Step 4: Output Enhanced Image using Eq. (6)

3.2.1. Common baseline

The 2-dimensional U-Net architecture is grounded on three major components, which are: an encoder, a decoder, and skip connections. The former utilizes convolutional layers to find image properties. After each layer, there is a max-pooling layer, reducing the input resolution by half. This reduction simplifies the convolutional operation so that we can obtain different features of an image at different resolutions of the input. The second component locates the regions of the blood vessels and optimizes the image resolution to the necessary input size. The up-sampling paths, which have the effect of scaling up the feature maps, are built with trainable deconvolutional layers to achieve better precision in prediction. During training, these layers will adjust to improve the accuracy of the segmentation masks. The third component, skip connections, helps significantly in refining decoder performance through the transfer of additional attributes of the image at each stage of the encoder. The last stage of the baseline model is the use of the softmax function, which produces a probability map,

which states that all the pixels are vessels or not. Finally, a segmentation mask is created by labeling pixels with a probability greater than 0.5 as a vessel (Siddique et al., 2021). Fig. 2 shows the conventional U-Net model. The depth of the whole network is chosen as 5, and skip connections link all levels of the encoder and decoder. In line with the standard structure of a Basic Layer Set (BLS)—which consists of a convolutional layer followed by a ReLU activation and batch normalization—each encoder level includes two BLS units along with a max-pooling layer. Similarly, every level of the decoder incorporates two BLS units and a single deconvolution layer. One BLS is positioned in the center of the encoder and the decoder, while the softmax function is employed to activate the final convolutional layer. This architecture, labeled as "B," is the baseline model for Spider U-Net.

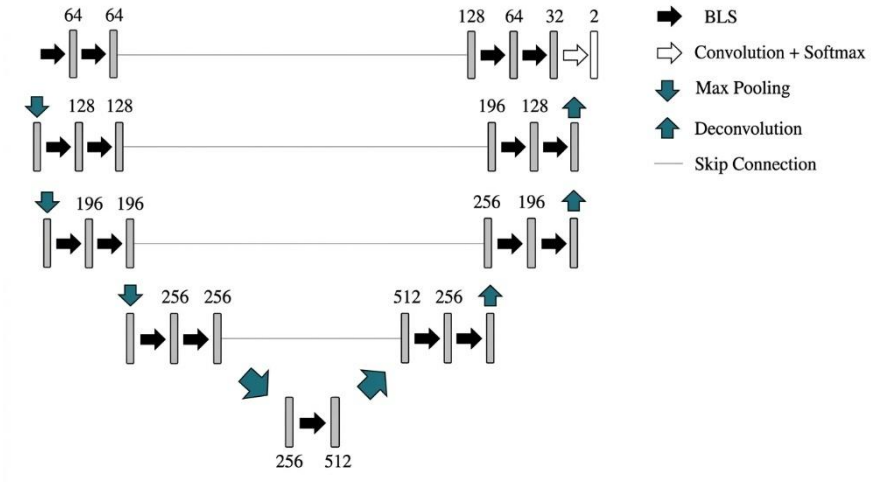


Fig. 2: Schematic diagram of the U-Net model (Jena et al., 2023)

3.2.2. Warp path (part A)

The warp path is constructed by aligning multiple instances of the baseline model B in parallel, with shared parameters, as illustrated in Fig. 1. This configuration allows the architecture to process and receive each slice in the image sequence is processed concurrently. The encoder component selects a collection of spatial attributes, displaying them next to each other, just like warp threads. On the other hand, the decoder block generates binary vessel segmentation masks by connectivity-aware spatial attributes with a supplemental warp path. Additional information on these operations is provided in the succeeding section.

The warp path is composed of T baseline units B, where T defines the model's input capacity—that is, the number of image sequence frames the model can process simultaneously. The value of T can be fixed arbitrarily by the network designer. Having T too high can be wasteful of two slices weaken with the distance among two slices increasing. To carry out pilot tests in several configurations and observed that a higher than five didn't improve the performance of the model.

3.2.3. Weft path (part B)

The weft path is created by changing the bottom-most convolutional layers that are located among the warp path's encoder and decoder with an individual bi-directional convolutional Long Short-Term Memory layer. This adjustment is intended to record inter-slice connectivity along the z-axis, as shown in Fig. 3. The use of a convolutional LSTM is intentional since the LSTM network family is optimized for rule and feature extraction from sequential data, guaranteeing stable contextual information retention via its internal memory units. Additionally, the convolutional Long Short-Term Memory can handle attributes from a CNN without losing spatial information, which is an important feature for semantic segmentation where inner operations are substituted by convolutional operations (Goni et al., 2022).

3.2.4. Data feeding strategy

To present an adapted data feeding strategy to Spider U-Net, referred to as "striding stencil (SS)," demonstrated in Fig. 4, to ensure stable and efficient training. Instead of working on the full sequence of images at once, SS invites Spider U-Net to work through data in multiple phases. First, Spider U-Net learns its architectural features from a subset of the volume, serving as an image order of length T, for the input capability of a pre-specified warp path. Second, the architecture proceeds using the inter-slice level according to a given natural number S. The two phases are repeated iteratively until the architecture proceeds through the whole volume. During the training phase, the value of S is defined to be less than T such that the ongoing image sequence overlaps to some extent with the earlier one. This intensive training fulfills two key roles: enhancing the data to prevent overfitting and ensuring the model's stability to the variance in the image sequence composition. At the inference stage, S is equated to T so that no two sequences of images overlap. The sparse inference approach offers high

time efficiency, making it the quickest technique for processing the entire volume. At the same time, dense training enables the model to consistently generate stable segmentation masks, regardless of variations within the image sequence.

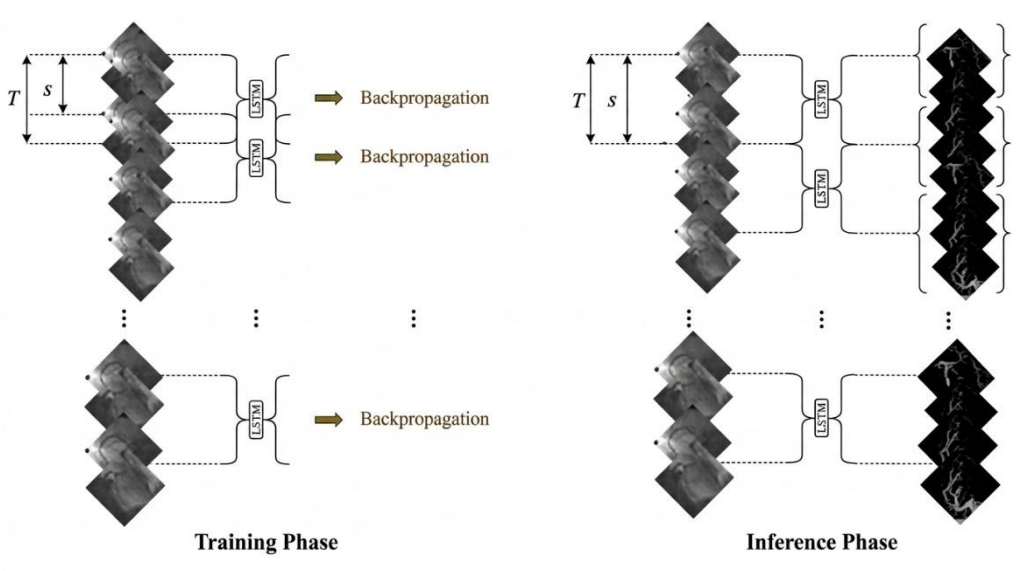


Fig. 3: The striding stencil is demonstrated for both the training and inference phases

4. Experimentation

4.1. Performance measures

In digital imaging, denoising and contrast enhancement approaches are evaluated using metrics like PSNR, RMSE, MSE, CoC (Wood, 2020), and NC. These provide objective comparisons between improved and true images.

PSNR (Peak Signal-to-Noise Ratio): Measures signal quality; greater values indicate better results (Kaur and Kaur, 2016).

$$\mathrm{PSNR} = 10 * \log_{10}((\mathrm{MAX}^2/\mathrm{MSE}) \quad (8)$$

MSE (Mean Squared Error): Computes the average squared error between the original and enhanced images. Lower is better (Kaur and Kaur, 2016).

$$\mathrm{MSE} = \left(\frac{1}{n*m}\right) * \sum\sum[(I(x,y) - D(x,y))^2] \quad (9)$$

RMSE (Root MSE): Square root of MSE; indicates average error (Khan et al., 2020; Khan et al., 2021).

$$\mathrm{RMSE} = \mathrm{sqrt}(\mathrm{MSE}) \quad (10)$$

CoC (Correlation Coefficient): Measures the similarity between original and enhanced image pixels.

$$\mathrm{CoC} = \mathrm{cov}(I, D)/(\sigma_I * \sigma_D) \quad (11)$$

NC (Normalization Coefficient): Evaluates contrast enhancement success.

$$\mathrm{NC} = (\mathrm{CE_A} - \mathrm{Org_B})/(\mathrm{CE_A} + \mathrm{Org_B}) \quad (12)$$

For vessel segmentation, measures such as Precision, Recall, Accuracy, F1-score, and Jaccard Similarity are applied.

These metrics help objectively assess the performance of image enhancement and segmentation methods. High PSNR, Precision, F1-score, and Jaccard indicate better results, while lower RMSE and MSE suggest fewer errors.

4.2. Results and discussion

The manuscript is predominantly devoted to the pre-processing and vessel segmentation applied on the images of coronary angiography with the view of improving the quality of the image by addressing the issues arising due to the low contrast, noise, and the segmentation of the coronary artery disease detectors. The study examines the various methods and their usefulness in enhancing the images prior to the identification of coronary artery diseases. This part is divided into three sub-categories, which are simulation setup, visual analysis, and statistical analysis.

4.3. Simulation setup

The simulation was carried out on a Windows 10 Pro computer, with the computation time quantified on a system with an Intel(R) Core(TM) i5-6300U CPU @ 2.40 GHz, 2.50 GHz, and 8GB RAM. The experiment applied JupyterLab, an open-source, web-based interactive IDE that is designed for computational modeling. Access to JupyterLab was made possible using an Anaconda environment. Anaconda provides a friendly environment for package management, dependency resolution, and code execution.

Dataset Description: Coronary angiography X-ray images (real-time X-ray imaging) were collected from two well-established medical institutions located in Peshawar, Pakistan: The cardiology center of Complex Hospital Hayatabad and the Teaching Hospital Khyber Peshawar. The images show the intricacy of coronary arteries with varied thicknesses and complex vascular structures against a background. In addition, the dataset contains examples of noise. All the images of a coronary artery in the dataset are 512 × 512 pixels in size. Angiographic image acquisition was done under the close observation and assistance of a radiologist. A total of 400 coronary angiogram images were collected for this study. The dataset was divided into two subsets, where 80% of the images were used for training purposes, and the remaining 20% were reserved for validation. These images were acquired using an angiographic imaging machine.

4.4. Visual analysis

Visual analysis plays an important role in assessing the effectiveness of image quality enhancement methods. For invasive coronary angiography or X-ray coronary angiography images, the images tend to be noisy and contain artifacts, as illustrated in Fig. 4. To overcome this limitation, advanced denoising techniques such as Median filter (MF) (Ning et al., 2009), Total Variation (TV) (Huang and Wan, 2020), Mean Filter (MEF) (Arulpandy and Pricilla, 2020), Modified Wiener Filter (MWF) (Park et al., 2020), Adaptive median filter (AMF) (Verma et al., 2015), and Weighted median filter (WMF) can be employed to enhance image clarity and reduce noise.

A region of interest (ROI) may be identified using red and green squares in order to compare the results of different denoising algorithms with the original image. This allows one to obtain a clear visual view of the noise-free images and the original image, and therefore, the individual can assess each method's performance in a detailed manner. The amplified images obtained through the selection of areas of the image allow a closer examination of the better quality of the image through the application of the techniques employed. The impact of the denoising techniques can be visually verified in a magnified picture of the areas of interest, with a more precise assessment of the improvement in image quality.

Fig. 5 shows the larger image that gives a close-up look at the denoised images obtained with the help of advanced denoising techniques. Such a validation process provides a deeper analysis of the performance of every method in enhancing the image quality by drawing comparisons between the details and sharpness of the areas highlighted as compared to the original image.

Through this verification process, it becomes evident whether the applied noise removal techniques successfully reduce noise and artifacts, leading to a visually improved representation of the angiography image.

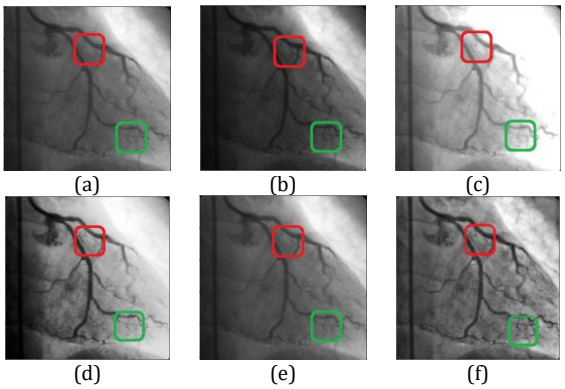


Fig. 4: Comparison of denoising techniques: (a) original noisy image; (b) MF; (c) TV; (d) MEF; (e) MWF; (f) AMF; and (g) WMF

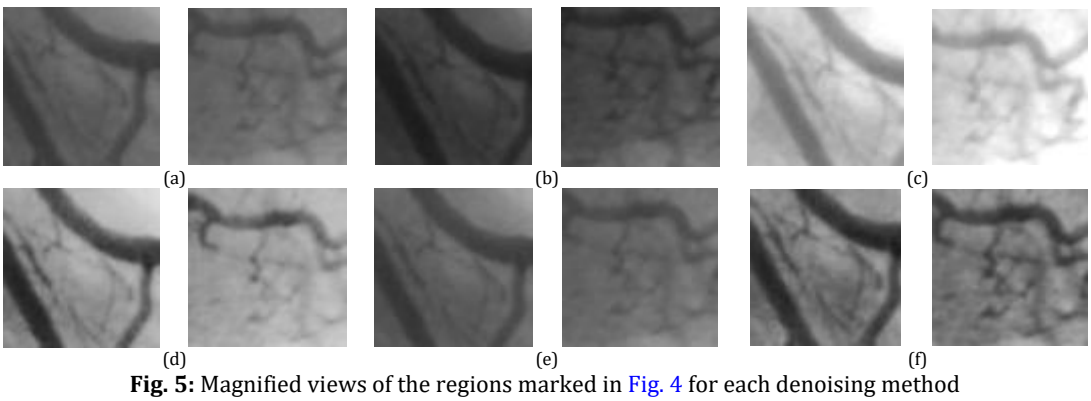


Fig. 5: Magnified views of the regions marked in Fig. 4 for each denoising method

Detecting low-contrast issues is crucial for digital images, particularly in the context of medical images. Fig. 6 presents a comparison of advanced image contrast techniques such as Contrast Stretching (CS)

(Showkat et al., 2021), Optimized Maximum Contrast (OMC) (Zhang et al., 2022), Local Transformation Histogram Equalization (LTHE), Histogram Equalization (HE) (Wang et al., 2020), Gamma Correction (GC) (Wang et al., 2020), Local Brightness Contrast (LBC) and Piecewise Linear Transformation (PLT) (Ibrahim et al., 2024) to determine the most appropriate approach for enhancing medical images. In Fig. 7, the modified image is annotated with red and green boxes, which effectively highlight the areas where the low contrast of the original image is identified. This comparison helps in identifying the specific technique that can effectively address the low contrast problem in medical images.

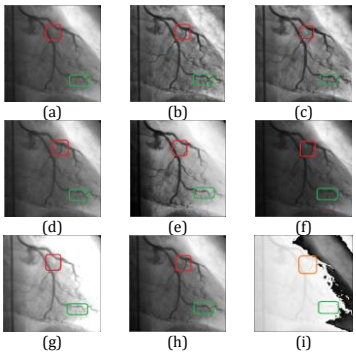


Fig. 6: Comparison of contrast enhancement techniques: (a) original image; (b) CS; (c) OMC; (d) LTHE; (e) HE; (f) GC; (g) LBC; (h) PLT; and (i) Sigmoid

In Figs. 4 and 6, noise reduction and contrast-improvement methods were separately employed for the input image. Fig. 7 displays the improved output images acquired by combining denoising and improving contrast methods. The procedure consists of first eliminating noise from the input image, resulting in a noise-free output image. This denoised image is then used as the input for contrast enhancement, with each contrast method combined with the denoising methods one by one.

After visual inspection of the images in Fig. 8, one can see that the initial two rows exhibit good results in combination with all the denoising methods, except for the last three rows, like LBC, PLT, and Sigmoid, which have poor results. In addition, looking at the first, third, and fifth columns, which are MF, MEF, and AMF in the same order, it is evident that when paired with all the contrast methods, it yields more efficient results than with other pairings.

As seen in Fig. 7, it is generally observed that some combinations, specifically those in rows 3 through 8, when paired with certain contrast enhancement techniques, fail to deliver satisfactory outcomes. This highlights the importance of thoughtfully selecting the appropriate pairing of denoising and contrast enhancement methods to achieve optimal image enhancement performance.

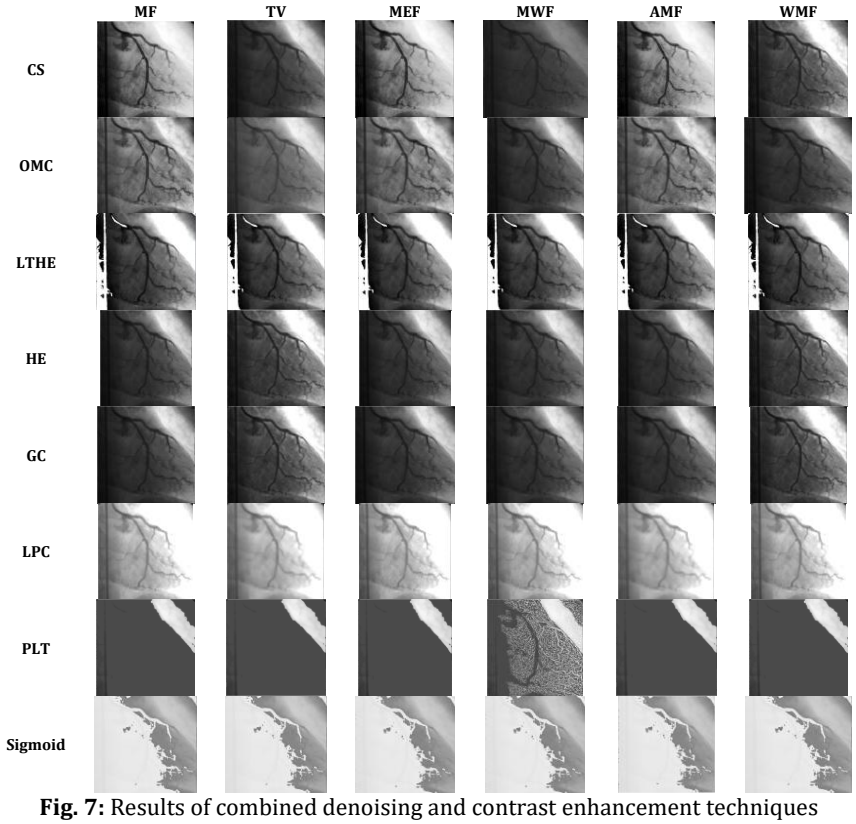


Fig. 7: Results of combined denoising and contrast enhancement techniques

To confirm the efficacy of the suggested architecture in conjunction with new noise removal and contrast enhancement hybrid methods (Preprocessing methods), and to give graphical comparisons in Figs. 8 and 9 employing sample test images from the test group. In Figs. 8 and 9, the suggested and conventional models, like U-Net and Spider U-Net architecture, respectively, are evaluated on both the original images (without pre-processing) and with our suggested hybrid methods.

The outcomes prove that our hybrid methods outperform true images in both the proposed and conventional models. In particular, the comparisons are between two hybrid methods: MF+OMC and AMF+OMC. Generally, both these methods have improvements over true images. Particularly, MF+OMC is always shown to be highly efficient, as seen in Figs. 8 and 9. The qualitative assessment and validation of the results were conducted by a cardiologist.

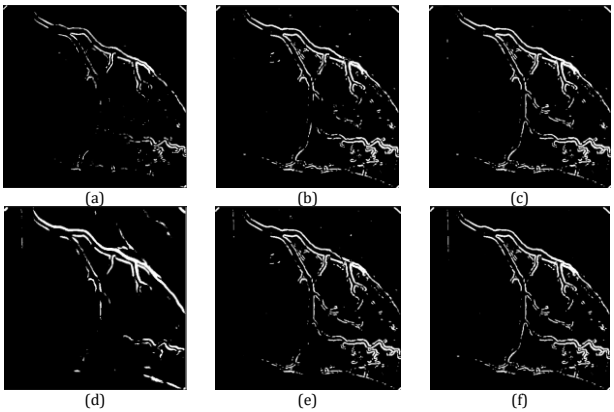


Fig. 8: Segmentation results for test image 1 using U-Net and Spider U-Net: (a, d) original images without preprocessing; (b, e) AMF+OMC; and (c, f) MF+OMC

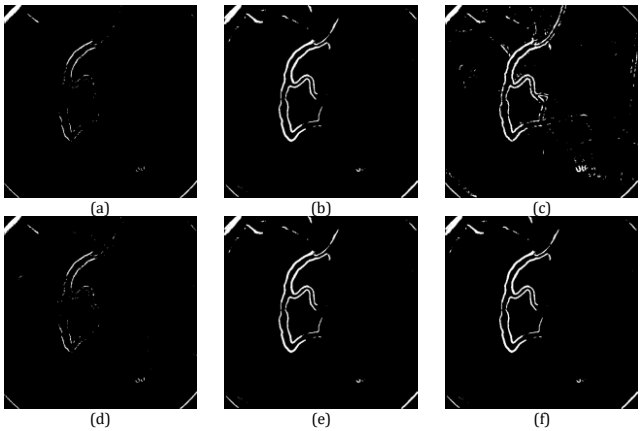


Fig. 9: Segmentation results for test image 2 using U-Net and Spider U-Net: (a, d) original images without preprocessing; (b, e) AMF+OMC; and (c, f) MF+OMC

4.5. Statistical analysis

In a statistical comparison of denoising methods, some popular measures of assessment are widely used. Performance comparison is based on the evaluation metrics: PSNR, MSE, NC, RMSE, and CoC. The comparison is done with the aim of testing the performance of the aforementioned approaches for enhancing the quality of denoised images.

Based on the data presented in Table 2, the PSNR values for the median filter, mean filter, and adaptive median filter techniques are recorded as 50.72, 49.15, and 47.00, respectively. These PSNR values are higher than those obtained with other applications such as TV, MWF, and WMF. The larger PSNR value implies that the median Filter technique is superior with regard to the removal of noise and the quality of the original image as compared to the other methods. That is, the denoised image created using the median Filter technique has a smaller amount of noise and is more comparable to the original image as compared to the denoised images created using the other techniques mentioned. In fact, the median Filter method has lower values of MSE and RMSE than the other methods, with values of 4.5509 and 0.7422, respectively; it is a better method of removing noise. MSE and RMSE are used to measure the mean squared error between values of corresponding pixels in the original and denoised images, which are used as measures of reconstruction accuracy.

The value of the correlation coefficient for the median filter and mean filter methods is close to 1, which means that the techniques show good outcomes in removing the noise and maintaining the original image structure and patterns. The correlation coefficient is a measure of the linear relationship between the pixel values of the true image and the denoised image. A value close to 1 means a strong positive correlation. The value of the

normalization coefficient of WMF is much higher than that of other methods in the specified scenario.

As indicated by the bold entries in Table 2, the median filter approach outperforms the other approaches under consideration in terms of its noise removal enhancement capabilities. The three most promising outcomes are further illustrated using distinct colors.

Table 2: Comparison among the advanced denoising methods

Methods	PSNR	MSE	RMSE	NC	CoC
Median filter	**50.72**	**4.5509**	**0.7422**	1.0542	**0.9998**
Total variation	35.15	72.2550	8.5002	1.1407	0.9954
Mean filter	49.15	5.8066	0.8981	**1.0827**	**0.9998**
Modified Wiener filter	34.87	765.0318	27.6592	1.0362	0.8973
Adaptive median filter	47.00	5.9811	0.9101	1.0000	0.9900
Weighted median filter	27.64	734.5465	27.0642	1.2178	0.1474

Based on the data presented in Table 3, the Optimized Maximum Contrast technique shows the highest PSNR value (34.92), indicating better preservation of image quality compared to the other techniques. The Optimized Maximum Contrast technique stands out with lower values for both MSE (22.4190) and RMSE (4.4616), which indicate desirable results. These measures quantify the average squared difference and the average magnitude of differences, respectively, between the original and contrast images.

The CoC value for the Contrast Stretching technique is closest to 1. Local Brightness Contrast exhibits a relatively high normalization coefficient value (1.2021), suggesting good preservation of image structure and patterns.

Table 3: Comparison among advanced contrast enhancement methods

Methods	PSNR	MSE	RMSE	NC	CoC
CS	34.42	23.4901	4.8466	1.1117	0.9999
OMC	34.92	22.4190	4.4616	1.0170	0.9939
LTHE	28.48	325.9286	18.0534	1.1513	0.9532
HE	28.04	1551.5836	39.3901	1.0224	0.9236
GC	27.71	1108.7820	33.2983	1.0965	0.9940
LBC	27.61	6108.1582	78.1547	1.2021	0.8751
PLT	27.96	189.7553	13.7751	1.0866	0.9921
Sigmoid	27.34	16059.9671	126.7279	1.0344	0.5996

Table 4 indicates the results that have been derived by amalgamating a combination of different denoising methods and contrast methods, which have been used in five different measures. For every contrast method, every noise removal method is used, and the statistical findings are indicated in depth. This research involves evaluating the three most effective contrast methods in reference to their performance as listed in Table 4. These are compared alongside various noise removal algorithms, including OMC, CS, and HE. In addition, the three best-performing denoising algorithms are selected from the results obtained: MF, MEF, and AMF.

A specific combination is found to be the best of all by the analysis. The median filter shows better results, especially when combined with different contrast methods. Interestingly enough, the OMC combined with the median filter gives outstanding results in comparison to all the other combinations. On the contrary, the OMC shows better results when mixed with the median filter. Our suggested method, MF+OMC, proves to be the better method out of all the combinations.

To analyze the performance of vessel segmentation of coronary angiogram images statistically. To report statistical comparisons in Table 5. In Table 5, two DL models, U-Net and Spider U-Net, are evaluated on the original images (free from any noise removal or contrast enhancement) and our proposed hybrid methods. In all tables, the color representation follows this pattern: dark green indicates the highest value, light green represents the second highest value, and a lighter shade of green denotes the third highest value.

5. Conclusion

The manuscript presents an effective framework for coronary artery disease (CAD) detection through the integration of advanced pre-processing techniques and deep learning-based vessel segmentation. The proposed hybrid preprocessing methods, including MF+OMC and AMF+OMC, significantly improved noise reduction and contrast enhancement, thereby enhancing the visual quality of coronary angiogram images. For vessel segmentation, the Spider U-Net architecture, an improved version of the traditional U-Net model, was employed. The incorporation of attention mechanisms enabled better feature extraction and more accurate localization of coronary vessels. Extensive experiments were conducted using both visual assessment and quantitative evaluation metrics, including PSNR, MSE, RMSE, normalization factor, correlation coefficient, accuracy, precision, recall, F1-score, and Jaccard index. Among the evaluated approaches, the MF+OMC method achieved superior performance across most evaluation metrics, demonstrating the effectiveness of the proposed framework. The overall results indicate that the proposed approach provides a reliable and efficient solution for coronary artery segmentation and CAD analysis in X-ray angiography images. The findings of this study may support clinical decision-making by improving the quality

and accuracy of coronary vessel analysis. In future work, the proposed framework can be extended toward real-time coronary vessel segmentation systems for clinical environments by integrating optimized deep learning models with high-performance computing platforms. Furthermore, future research may investigate the applicability of the proposed pre-processing and segmentation framework to other medical imaging modalities, such as CT angiography and MRI, as well as evaluate the framework on larger and more diverse clinical datasets.

Table 4: Summary of results for combined denoising and contrast enhancement techniques

Contrast methods	Denoising methods	PSNR	MSE	RMSE	NC	CoC
Contrast stretching	MF	28.71	1109.4029	33.3077	1.1921	0.9467
	TV	27.59	13944.7658	118.0879	1.1022	0.9371
	MEF	28.75	1110.2374	33.3202	1.2092	0.9261
	MWF	27.34	1164.7641	34.1286	1.9907	0.8296
	AMF	28.74	1110.8764	33.3298	1.2053	0.9392
	WMF	26.91	1142.9572	35.8281	1.1023	0.7311
Optimized maximum contrast	MF	29.58	398.1606	19.9539	7.3002	0.9358
	TV	27.59	13119.8093	114.5417	7.2978	0.9278
	MEF	28.68	373.4837	19.3257	7.2984	0.9377
	MWF	27.58	401.3237	21.8720	7.2924	0.9177
	AMF	28.45	400.1249	20.0031	7.3225	0.9195
	WMF	27.41	621.2374	29.6472	5.6900	0.8260
Local transformation histogram equalization	MF	27.82	1388.3671	36.8489	1.1569	0.9335
	TV	27.65	13888.3953	117.8490	3.3385	0.7195
	MEF	27.88	1584.5242	39.8495	1.1553	0.9375
	MWF	27.81	11888.5242	108.8495	1.0264	0.9182
	AMF	27.34	1488.8909	37.8468	1.1649	0.9334
	WMF	26.18	12875.9101	111.7960	1.0010	0.9102
Histogram equalization	MF	27.98	1551.7998	39.3928	1.0689	0.9235
	TV	27.59	1944.7658	50.7658	1.0765	0.9210
	MEF	27.96	1553.0809	39.4091	1.0961	0.9233
	MWF	27.16	1882.8712	47.7323	1.0321	0.9201
	AMF	27.90	1552.5106	39.4019	1.0982	0.9235
	WMF	27.85	1734.7823	42.7539	0.9874	0.9192
Gamma correction	MF	27.60	4121.4227	64.1983	1.0980	0.9937
	TV	27.54	13944.7658	118.0879	0.9887	0.9911
	MEF	27.55	4117.9313	64.1911	1.0981	0.9938
	MWF	27.48	20610.3674	143.5631	1.1085	0.9894
	AMF	27.50	4143.3501	64.3688	1.0986	0.9934
	WMF	27.37	4623.9982	68.9211	1.0920	0.9788
Local brightness contrast	MF	27.79	7026.7845	83.8259	1.2019	0.8740
	TV	26.75	13727.2247	117.1632	11.0927	0.9983
	MEF	27.87	7028.7331	83.8375	1.2196	0.8741
	MWF	27.01	8298.8772	86.9211	1.1002	0.7942
	AMF	27.72	13840.4137	117.6452	10.9067	0.9936
	WMF	26.91	8219.5427	85.2811	1.2910	0.8421
Piecewise linear transformation	MF	27.60	1386.7931	37.2396	1.2020	0.8794
	TV	27.58	13889.0230	117.8516	7.2677	0.8160
	MEF	27.12	1388.1697	37.2581	1.1972	0.8791
	MWF	27.39	4024.3141	63.4374	1.1839	0.5417
	AMF	27.75	1384.9427	37.2148	1.1934	0.7796
	WMF	27.32	4982.8711	70.4738	1.1022	0.8463
Sigmoid	MF	27.62	14940.9744	122.2332	1.1627	0.8780
	TV	27.06	4066.6905	63.7706	2.3061	0.8382
	MEF	27.60	14946.8369	122.2572	1.1567	0.8384
	MWF	27.38	4372.9372	68.1202	1.1022	0.7834
	AMF	27.64	14941.0499	122.2335	1.1692	0.8581
	WMF	26.91	3023.4822	49.9112	1.1231	0.7372

Table 5: Statistical comparison between the proposed and existing approaches for coronary angiogram analysis

Segmented model	Proposed methods	Accuracy	F1-score	Jaccard similarity	Recall	Precision
U-Net model	MF+OMC	0.9232	0.8491	0.7675	0.9118	0.7619
	AMF+OMC	0.8782	0.7755	0.7545	0.9125	0.7348
	Original image	0.7721	0.7250	0.6250	0.6250	0.7100
Spider U-Net model	MF+OMC	0.9549	0.8510	0.7836	0.9008	0.8762
	AMF+OMC	0.8715	0.8016	0.7558	0.8922	0.8034
	Original image	0.8221	0.7127	0.6126	0.8126	0.7600

List of abbreviations

3D	Three-dimensional
AI	Artificial intelligence
AMF	Adaptive median filter
AMF+OMC	Adaptive median filter with optimized maximum contrast
BLS	Basic layer set
CAD	Coronary artery disease
CDF	Cumulative distribution function
CNN	Convolutional neural network
CoC	Correlation coefficient
CPU	Central processing unit
CS	Contrast stretching
CT	Computed tomography
Dense Net	Densely connected convolutional network
DL	Deep learning
GC	Gamma correction
HE	Histogram equalization
IDE	Integrated development environment
LBC	Local brightness contrast
LSTM	Long short-term memory
LTHE	Local transformation histogram equalization
MEF	Mean filter
MF	Median filter
MF+OMC	Median filter with optimized maximum

	contrast
MRI	Magnetic resonance imaging
MSE	Mean squared error
MSSIM	Mean structural similarity index measure
MWF	Modified Wiener filter
NAE	Normalized absolute error
NC	Normalization coefficient
OMC	Optimized maximum contrast
PLT	Piecewise linear transformation
PSNR	Peak signal-to-noise ratio
ReLU	Rectified linear unit
ResNet	Residual network
RMSE	Root mean squared error
ROI	Region of interest
SNR	Signal-to-noise ratio
SS	Striding stencil
SSIM	Structural similarity index measure
T-Net	Transformation network
TV	Total variation
U-Net	U-shaped convolutional neural network architecture
VGG-16	Visual geometry group 16-layer network
VSSC-Net	Vessel specific skip connection network
WMF	Weighted median filter

Compliance with ethical standards

Conflict of interest

The author(s) declared no potential conflicts of interest with respect to the research, authorship, and/or publication of this article.

References

Agarwal M, Rani G, and Dhaka VS (2020). Optimized contrast enhancement for tumor detection. International Journal of Imaging Systems and Technology, 30(3): 687-703. https://doi.org/10.1002/ima.22408

Arulpandy P and Pricilla MT (2020). Speckle noise reduction and image segmentation based on a modified mean filter. Computer Assisted Methods in Engineering and Science, 27(4): 221-239.

Balasamy K and Shamia D (2023). Feature extraction-based medical image watermarking using fuzzy-based median filter. IETE Journal of Research, 69(1): 83-91. https://doi.org/10.1080/03772063.2021.1893231

Chen BQ, Cui JG, Xu Q, Shu T, and Liu HL (2019). Coupling denoising algorithm based on discrete wavelet transform and modified median filter for medical image. Journal of Central South University, 26: 120-131. https://doi.org/10.1007/s11771-019-3987-9

Dar KA and Mittal S (2021). An enhanced adaptive histogram equalization based local contrast preserving technique for HDR images. IOP Conference Series: Materials Science and Engineering, 1022(1): 012119. https://doi.org/10.1088/1757-899X/1022/1/012119

Goni MR, Ruhaiyem NIR, Mustapha M, Achuthan A, and Nassir CMNCM (2022). Brain vessel segmentation using deep learning—A review. IEEE Access, 10: 111322-111336. https://doi.org/10.1109/ACCESS.2022.3214987

Hao D, Ding S, Qiu L, Lv Y, Fei B, Zhu Y, and Qin B (2020). Sequential vessel segmentation via deep channel attention network. Neural Networks, 128: 172-187. https://doi.org/10.1016/j.neunet.2020.05.005 **PMid:32447262 PMCid:PMC8681868**

He K, Zhang X, Ren S, and Sun J (2016). Deep residual learning for image recognition. In the 2016 IEEE Conference on Computer Vision and Pattern Recognition (CVPR), IEEE, Las Vegas, USA: 770-778. https://doi.org/10.1109/CVPR.2016.90 **PMid:26180094**

Huang G, Liu Z, Van Der Maaten L, and Weinberger KQ (2017). Densely connected convolutional networks. In 2017 IEEE Conference on Computer Vision and Pattern Recognition (CVPR), IEEE, Honolulu, USA: 2261-2269. https://doi.org/10.1109/CVPR.2017.243

Huang S and Wan S (2020). A total variation denoising method based on median filter and phase consistency. Sensing and Imaging, 21: 19. https://doi.org/10.1007/s11220-020-00281-8

Huang W, Huang L, Lin Z, Huang S, Chi Y, Zhou J, Zhang J, Tan RS, and Zhong L (2018). Coronary artery segmentation by deep learning neural networks on computed tomographic coronary angiographic images. In the 40th Annual International Conference of the IEEE Engineering in Medicine and Biology Society (EMBC), IEEE, Honolulu, USA: 608-611. https://doi.org/10.1109/EMBC.2018.8512328

Ibrahim H, Mohamed AENA, Ammar R, El-Hag NA, Abou-Elazm A, Abd El-Samie FE, El-Shafai W, and Elsafrawey A (2024). Efficient color image enhancement using piecewise linear transformation and gamma correction. Journal of Optics, 53: 2027-2037. https://doi.org/10.1007/s12596-023-01171-4

Jena B, Jain S, Nayak GK, and Saxena S (2023). Analysis of depth variation of U-Net architecture for brain tumor segmentation. Multimedia Tools and Applications, 82: 10723-10743. https://doi.org/10.1007/s11042-022-13730-1

Jun TJ, Kweon J, Kim YH, and Kim D (2020). T-Net: Nested encoder–decoder architecture for the main vessel segmentation in coronary angiography. Neural Networks, 128: 216-233. https://doi.org/10.1016/j.neunet.2020.05.002 **PMid:32447265**

Kaur R and Kaur S (2016). Comparison of contrast enhancement techniques for medical image. In the 2016 Conference on Emerging Devices and Smart Systems (ICEDSS), IEEE, Namakkal, India: 155-159. https://doi.org/10.1109/ICEDSS.2016.7587782 **PMCid:PMC4946872**

Khan SS, Khan M, Alharbi Y, Haider U, Ullah K, and Haider S (2021). Hybrid sharpening transformation approach for multifocus image fusion using medical and nonmedical images. Journal of Healthcare Engineering, 2021: 7000991. https://doi.org/10.1155/2021/7000991 **PMid:34931139 PMCid:PMC8684527**

Khan SS, Khan M, and Alharbi Y (2020). Multi focus image fusion using image enhancement techniques with wavelet transformation. International Journal of Advanced Computer Science and Applications, 11(5): 414–420. https://doi.org/10.14569/IJACSA.2020.0110555

Khan SS, Khan M, and Alharbi Y (2023a). Fast local Laplacian filter based on modified Laplacian through bilateral filter for coronary angiography medical imaging enhancement. Algorithms, 16(12): 531. https://doi.org/10.3390/a16120531

Khan SS, Khan M, and Khan RS (2023b). Automatic segmentation and classification to diagnose coronary artery disease (AuSC-CAD) using angiographic images: a novel framework. In the 2023 18th International Conference on Emerging Technologies (ICET), IEEE, Peshawar, Pakistan: 110-115. https://doi.org/10.1109/ICET59753.2023.10374634

Lee K, Sunwoo L, Kim T, and Lee KJ (2021). Spider U-Net: Incorporating inter-slice connectivity using LSTM for 3D blood vessel segmentation. Applied Sciences, 11(5): 2014. https://doi.org/10.3390/app11052014

Ma Y, Hua Y, Deng H, Song T, Wang H, Xue Z, Cao H, Ma R, and Guan H (2021). Self-supervised vessel segmentation via adversarial learning. In the 2021 IEEE/CVF International Conference on Computer Vision (ICCV), IEEE, Montreal,

Canada: 7516-7525. https://doi.org/10.1109/ICCV48922.2021.00744

Ning CY, Liu SF, and Qu M (2009). Research on removing noise in medical image based on median filter method. In the 2009 IEEE International Symposium on IT in Medicine & Education, IEEE, Jinan, China: 384-388. https://doi.org/10.1109/ITIME.2009.5236393

Park CR, Kang SH, and Lee Y (2020). Median modified Wiener filter for improving the image quality of gamma camera images. Nuclear Engineering and Technology, 52(10): 2328-2333. https://doi.org/10.1016/j.net.2020.03.022

Sagar P, Upadhyaya A, Mishra SK, Pandey RN, Sahu SS, and Panda G (2020). A circular adaptive median filter for salt and pepper noise suppression from MRI images. Journal of Scientific & Industrial Research, 79(10): 941–944. https://doi.org/10.56042/jsir.v79i10.43588

Samuel PM and Veeramalai T (2021). VSSC Net: Vessel specific skip chain convolutional network for blood vessel segmentation. Computer Methods and Programs in Biomedicine, 198: 105769. https://doi.org/10.1016/j.cmpb.2020.105769 **PMid:33039919**

Showkat S, Parah SA, and Gull S (2021). Embedding in medical images with contrast enhancement and tamper detection capability. Multimedia Tools and Applications, 80: 2009-2030. https://doi.org/10.1007/s11042-020-09732-6

Siddique N, Paheding S, Elkin CP, and Devabhaktuni V (2021). U-Net and its variants for medical image segmentation: A review of theory and applications. IEEE Access, 9: 82031-82057. https://doi.org/10.1109/ACCESS.2021.3086020

Thuy LNL, Trinh TD, Anh LH, Kim JY, Hieu HT, and Bao PT (2021). Coronary vessel segmentation by coarse-to-fine strategy using U-nets. BioMed Research International, 2021: 5548517. https://doi.org/10.1155/2021/5548517 **PMid:33898624 PMCid:PMC8052146**

Verma K, Singh BK, and Thoke AS (2015). An enhancement in adaptive median filter for edge preservation. Procedia Computer Science, 48: 29-36. https://doi.org/10.1016/j.procs.2015.04.106

Vilimek D, Kubicek J, Golian M et al. (2022). Comparative analysis of wavelet transform filtering systems for noise reduction in ultrasound images. PLOS ONE, 17(7): e0270745. https://doi.org/10.1371/journal.pone.0270745 **PMid:35797331 PMCid:PMC9262246**

Wang C, Liu W, and Jimenez G (2020). Using chaos world cup optimization algorithm for medical images contrast enhancement. Concurrency and Computation: Practice and Experience, 32(5): e5482. https://doi.org/10.1002/cpe.5482

Wang F, Jiang M, Qian C, Yang S, Li C, Zhang H, Wang X, and Tang X (2017). Residual attention network for image classification. In the 2017 IEEE Conference on Computer Vision and Pattern Recognition (CVPR), IEEE, Honolulu, USA: 6450-6458. https://doi.org/10.1109/CVPR.2017.683

Wood ML (2020). Variability and standardization of quantitative imaging. Investigative Radiology, 55(9): 617-618. https://doi.org/10.1097/RLI.0000000000000667 **PMid:32776768**

Xian Z, Wang X, Yan S, Yang D, Chen J, and Peng C (2020). Main coronary vessel segmentation using deep learning in smart medical. Mathematical Problems in Engineering, 2020: 8858344. https://doi.org/10.1155/2020/8858344

Zhang W, Zhuang P, Sun HH, Li G, Kwong S, and Li C (2022). Underwater image enhancement via minimal color loss and locally adaptive contrast enhancement. IEEE Transactions on Image Processing, 31: 3997-4010. https://doi.org/10.1109/TIP.2022.3177129 **PMid:35657839**